Pramana – J. Phys. (2020) 94:5
https://doi.org/10.1007/s12043-019-1866-4

Improvement of transconductance and cut-off frequency in $In_{0.1}Ga_{0.9}N$ back-barrier-based double-channel $Al_{0.3}Ga_{0.7}N/GaN$ high electron mobility transistor by enhancing the drain source contact length ratio

RACHITA MOHAPATRA and PRADIPTA DUTTA*

School of Electronics Engineering, Kalinga Institute of Industrial Technology Deemed to be University, Bhubaneswar 751 024, India
*Corresponding author. E-mail: cr_dutta@yahoo.com

MS received 29 April 2019; revised 15 August 2019; accepted 21 August 2019

Abstract. An aluminium gallium nitride/gallium nitride ($Al_{0.3}Ga_{0.7}N/GaN$) high electron mobility transistor (HEMT) is designed at a gate length (L_G) of 0.1 μm, drain-to-source spacing (L_{SD}) of 3 μm and drain length to source length ratio (L_D:L_S) of 1. The HEMT is investigated by considering four different heterostructures, namely single channel, single channel with back-barrier, double channel and double channel with back-barrier. A two-dimensional electron gas (2DEG) is formed at the interface of AlGaN/GaN HEMT (DC HEMT). The physical importance of indium gallium nitride (InGaN) as back-barrier is to increase carrier confinement by raising the conduction band of GaN buffer. The double-channel HEMT (DC HEMT) with back-barrier shows the highest current drive. There is an improvement of 3.16% in drain current and an improvement of 4.58% in cut-off frequency at a gate-to-source voltage of -0.5 V for the DC HEMT with back-barrier compared to the DC HEMT without back-barrier. For further improvement in transconductance and cut-off frequency, the structure of DC HEMT with back-barrier is modified by increasing the drain contact length and decreasing the source contact length, that is L_D:$L_S = 3$, keeping the drain-to-source spacing unchanged, i.e. $L_{SD} = 3$ μm. There is 32.55% improvement in transconductance and 14.03% improvement in cut-off frequency at a gate-to-source voltage of -0.5 V for the DC HEMT with back-barrier at L_D:$L_S = 3$ compared to the DC HEMT with back-barrier at L_D:$L_S = 1$.

Keywords. High electron mobility transistor; back-barrier; two-dimensional electron gas; heterostructures.

PACS No. 85.30.–z

1. Introduction

Modern digital communication system mainly depends on the RF performances regarding bandwidth, efficiency and output power. Silicon technology is dominant in the semiconductor industry as it plays a key role in downscaling of devices but silicon-based devices are approaching the maximum limit of operation and are not able to deliver the performance required by future microwave and RF applications. So research is going on to replace the silicon technology by silicon carbide (SiC), silicon–germanium alloy (SiGe) and group III–V semiconductors. The gallium arsenide (GaAs) metal semiconductor field effect transistors (MESFETs) operate at good range of frequencies because of their high carrier mobility but their electrical conductance is one-third of that of silicons, and so they are used in low power applications [1]. SiC MESFETs are used in high-voltage and high-temperature applications but they are incapable of forming heterostructures, and so they have low electron mobility and operates at low frequencies [2]. The group-III nitrides have wide band gaps and exist in wurtzite crystal structure that give rise to polarisation effects and the electron gas formed due to polarisation has high carrier mobility, and so they are used in high-frequency and high-power applications [3].

Among the group-III nitrides, gallium nitrides (GaN) exhibits very strong piezoelectric polarisation which is due to the mechanical strain in the material [4]. Spontaneous polarisation is due to crystal asymmetry that results in the repulsion of geometric centres of positive charge and negative charge to form a dipole [5]. GaN is the best nitride among all the group-III nitrides due to its superior performance in RF applications [6]. The

Published online: 18 December 2019

band gap of GaN is 3.24 eV that helps to resist high temperature and high electric field [6]. The sheet charge density of electron gas formed in the triangular well at the heterojunction is nearly 10^{12} to 10^{13} cm^{-2} [7]. The mobility of the electrons in the two-dimensional electron gas (2DEG) is high as they suffer less Coulomb scattering while travelling in the channel. So, the cut-off frequencies of these devices are high and used for high-frequency applications. The dielectric constant for GaN is 9.0 which is less than 11.8 which is the dielectric constant for silicon, and so the junction capacitances for gallium nitride high electron mobility transistors (GaN HEMTs) is also less.

Intentional doping is not required in GaN HEMTs to operate as the electron gas formed for conduction in HEMTs is due to piezoelectric and spontaneous polarisation. GaN has a high saturation velocity of 3×10^7 cm/s, and so the current saturation level is high [8]. The output power performance of GaN HEMTs has reached outstanding values in the last years [9]. Though GaN HEMT provides high frequencies, at k-band more high-frequency operation is required for which the gate length should be reduced but scaling down the devices reduces the confinement of 2DEG [10]. To increase the confinement of electrons and for better device performances, an InGaN back-barrier is placed below the AlGaN layer [11]. InGaN facilitates to grow good quality materials with less traps and helps in improving interface and surface roughness [12,13]. There is improvement in DC and RF performances on the use of back-barrier. However, as InGaN is a low band-gap material there is reduced breakdown voltage for which the devices give a low output power. At higher frequencies, the output current swing of single-channel HEMTs (SC HEMTs) decreases due to current collapse resulting from trapping and detrapping of the surface states near the gate-drain region [14,15].

DC HEMTs are used to increase the output current but they suffer from poor gate control for the lower channel. So a proper construction of the HEMT helps to overcome the problem [16]. For more improvement in electron confinement and reduced carrier scattering for the lower channel, a DC HEMT with InGaN back-barrier is designed. A DC AlGaN/GaN HEMT with back-barrier that gives high output power is reported [17]. However, the device is further modified to get improved transconductance and cut-off frequency by increasing the drain contact length and reducing the source contact length, that is L_D:$L_S = 3$, keeping the drain-to-source distance (L_{SD}) of 3 μm constant so that the parasitic capacitances and resistances remain unchanged [18]. In §2 the device description of single channel (SC), single channel with back-barrier (SC with back-barrier), double channel (DC) and double channel with back-barrier (DC with back-barrier) is presented. DC and RF analysis of all the heterostructures are presented in §3 and finally the conclusion is given in §4.

2. Structure specification and materials used

Figure 1a represents the SC AlGaN/GaN HEMT with AlGaN as the channel layer with n-type doping of 2×10^{18} cm^{-3} and thickness of 20 nm. GaN is the substrate layer with 1.5 μm thickness. Fabrication of AlGaN/GaN HEMTs on Si, SiC or sapphire substrates leads to increased mismatch with GaN layer which results in threading dislocations [19]. Presence of dislocations reduces carrier mobility, increases leakage current and results in early breakdown of the device. Though GaN substrates are expensive, they provide reduced lattice mismatch and low dislocation density [20]. The gate length (L_G) is 0.1 μm, drain length (L_D) is 1.0 μm, source length (L_S) is 1.0 μm, the gate-to-source length (L_{GS}) is 0.9 μm and the gate-to-drain length (L_{GD}) is 2 μm. The gate-to-drain spacing is more than gate-to-source spacing as increase in gate-to-drain spacing reduces the electric field near the gate–drain region and improves the breakdown voltage of the device. The gate has a Schottky contact with a barrier of 1.1 eV. The drain and source are heavily doped regions so that they form ohmic contacts. The device is passivated to protect it from moisture and contaminants. Silicon nitride (SiN) is used as the passivation layer. The passivation layer also reduces Fermi level pinning [21]. A 2DEG is formed at the heterojunction of AlGaN and GaN layers. The charges formed at the interfaces due to piezoelectric and spontaneous polarisation are calculated and used in simulations [22,23].

Figure 1b represents the SC HEMT with back-barrier. The back-barrier used is indium gallium nitride ($In_{0.1}Ga_{0.9}N$) of 4 nm thickness. It prevents current injection into the buffer and reduces scattering of electrons thereby increasing the electron density [9].

Figure 1c represents the DC HEMT. A lower $Al_{0.06}Ga_{0.94}N$ barrier layer of 17 nm thickness is used. DC HEMTs suffer from poor gate control for the lower channel and so a proper construction of the HEMT, i.e. use of lower AlGaN layer of less aluminium composition and small thickness is used in this structure to overcome the problem. To improve electron density and to make good ohmic contacts, the upper barrier is selectively doped. Two channels are formed at the top and bottom AlGaN/GaN interfaces. One of the channel is formed at 20 nm and the other at 51 nm.

Figure 1d represents the DC HEMT with back-barrier (DC with back-barrier). The back-barrier used is InGaN with 4 nm thickness. The back-barrier raises the

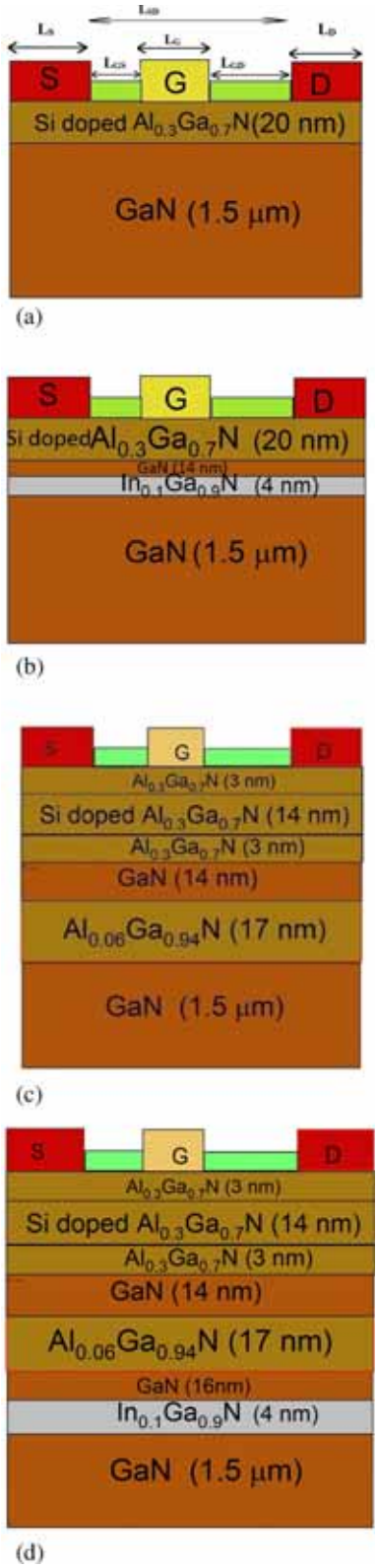

Figure 1. Heterostructures. (**a**) Single-channel AlGaN/GaN HEMT, (**b**) single-channel AlGaN/GaN HEMT with back-barrier (SC with back-barrier), (**c**) double-channel AlGaN/GaN HEMT and (**d**) double-channel AlGaN/GaN HEMT with back-barrier (DC with back-barrier).

conduction band of the GaN buffer with respect to the channel to increase confinement of electrons.

3. Simulated results

In this section, DC and RF analyses are done to obtain the drain current (I_{DS}), transconductance (g_m), gate-to-source capacitance (C_{GS}), gate-to-drain capacitance (C_{GD}) and cut-off frequency (f_T) for all the heterostructures.

Table 1 shows the mobility of all the heterostructures. The low-field electron mobility is calculated using Arora model and high field electron mobility is calculated using the transferred electron effect-2 model [24]. The mobility decreases on inserting a back-barrier.

Figure 2 represents the I_{DS}–V_{GS} graphs for SC AlGaN/GaN HEMT on GaN and Si substrates. It is observed that the drain current is more in the case of HEMT on GaN substrate because when GaN substrate is used lattice mismatch is reduced and output drain current increases. The maximum drain current obtained at $V_{DS} = 10$ V is 3.48 and 2.68 mA/μm for HEMT on GaN and Si substrates respectively. Figure 3 shows I_{DS}–V_{DS} graph for all the heterostructures. It is seen that the drain current increases for DC HEMT and it

Table 1. Mobility of heterostructures.

Sructures	Mobility (cm^2/Vs)
SC HEMT	1070
SC HEMT with back-barrier	990
DC HEMT	1090
DC HEMT with back-barrier	1050

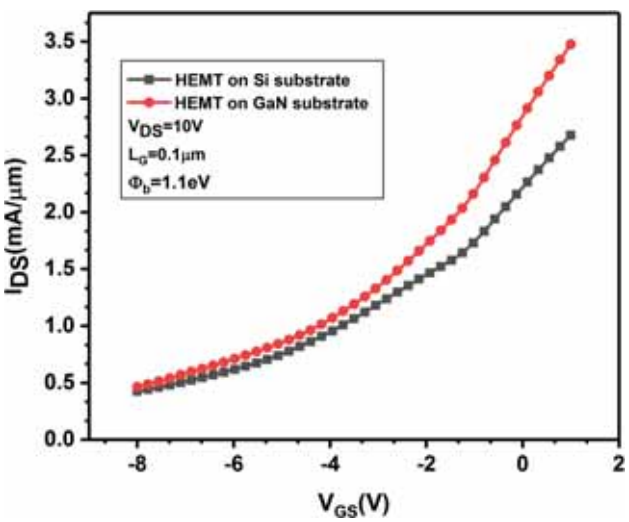

Figure 2. I_{DS}–V_{GS} graph for the SC AlGaN/GaN HEMT on Si and GaN substrates at $V_{DS} = 10$ V.

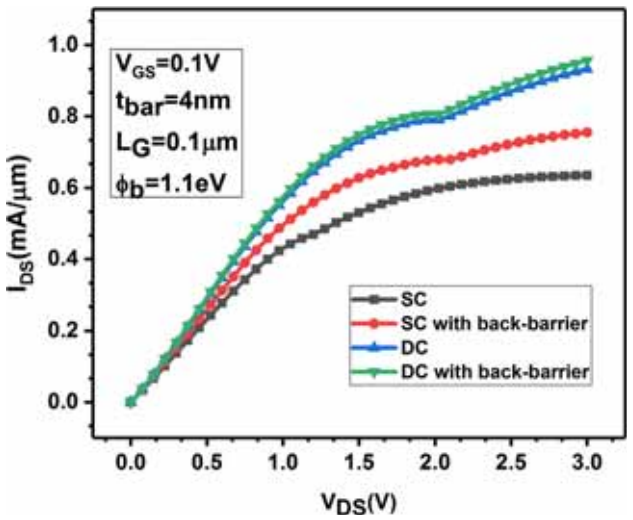

Figure 3. I_{DS}–V_{DS} graph for the heterostructures at $V_{GS} = 0.1$ V.

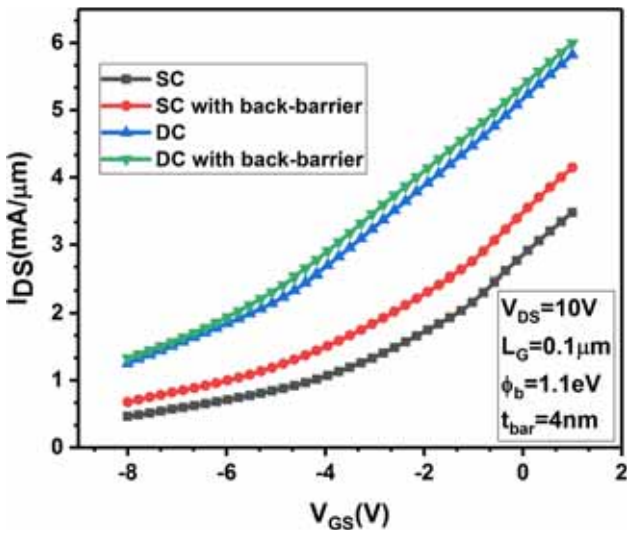

Figure 4. I_{DS}–V_{GS} graph for the heterostructures at $V_{DS} = 10$ V.

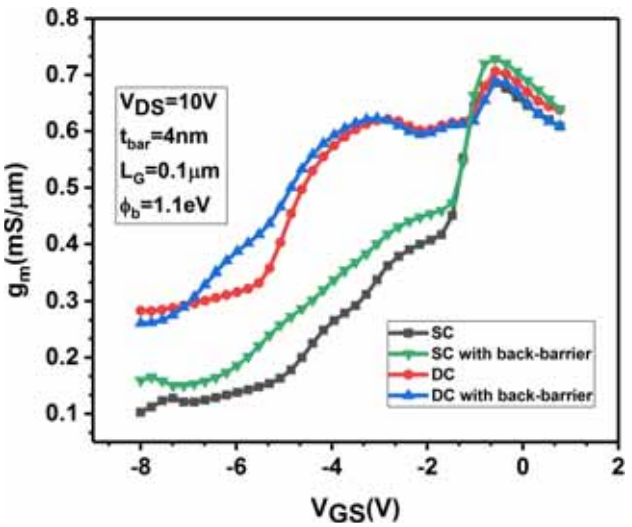

Figure 5. g_m–V_{GS} graph for the heterostructures at $V_{DS} = 10$ V.

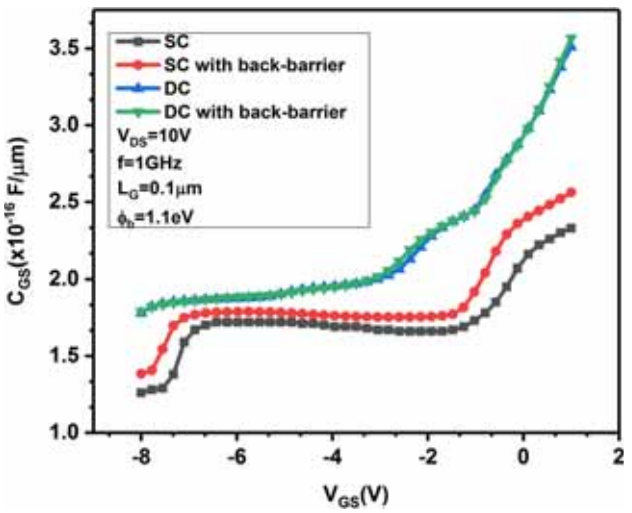

Figure 6. C_{GS}–V_{GS} graph for the heterostructures at $f = 1$ GHz.

further increases when a back-barrier is used. In DC HEMTs, polarisation induces two channels and so current drive is high. The back-barrier increases the electron confinement and prevent leakage of current to the buffer. The maximum drain current for DC with back-barrier is 0.95 mA/μm when $V_{GS} = 0.1$ V.

Figure 4 represents the I_{DS}–V_{GS} graph for all the heterostructures. The electron density of the single channel increases when a back-barrier is used and it further increases when a DC HEMT is used. In DC HEMT, two channels are formed at the interface of AlGaN/GaN and the electron confinement of the lower channel is increased by introducing a back-barrier that increases the output current. The maximum drain current for DC with back-barrier is 6 mA/μm when $V_{DS} = 10$ V.

Figure 5 depicts the transconductance graph for different heterostructures. It is observed that a double hump structure is formed for the DC HEMTs because of modulation of the upper and lower channels formed at the interfaces of AlGaN/GaN. The transconductance slightly decreases for DC HEMTs compared to SC HEMTs because the gate control for the lower channel decreases in the case of DC HEMTs [25]. When a back-barrier is used in SC HEMT, the transconductance improves because the electron confinement improves and better modulation of electrons by gate voltage is obtained at high drain voltage. The maximum transconductance for DC with back-barrier is 0.68 mS/μm when $V_{DS} = 10$ V.

Figure 6 shows the C_{GS}–V_{GS} graph for all the heterostructures at $V_{DS} = 10$ V. Figure 7 shows the

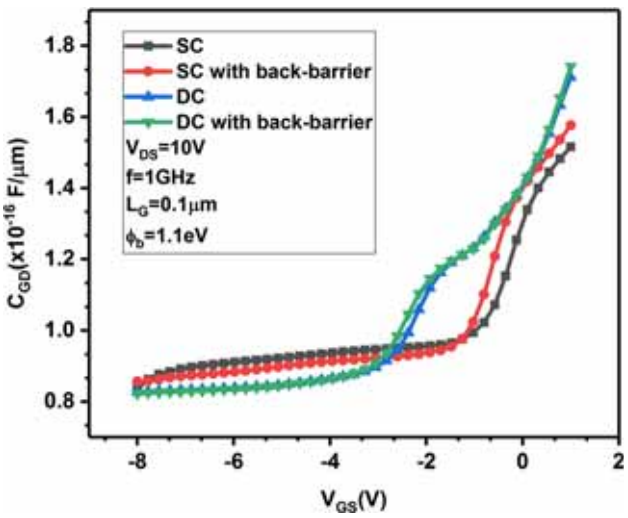

Figure 7. C_{GD}–V_{GS} graph for the heterostructures at $f = 1$ GHz.

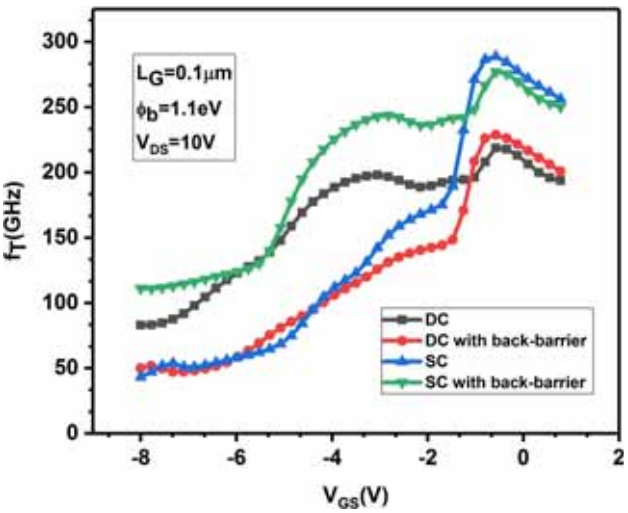

Figure 8. f_T–V_{GS} graph for the heterostructures at $V_{DS} = 10$ V.

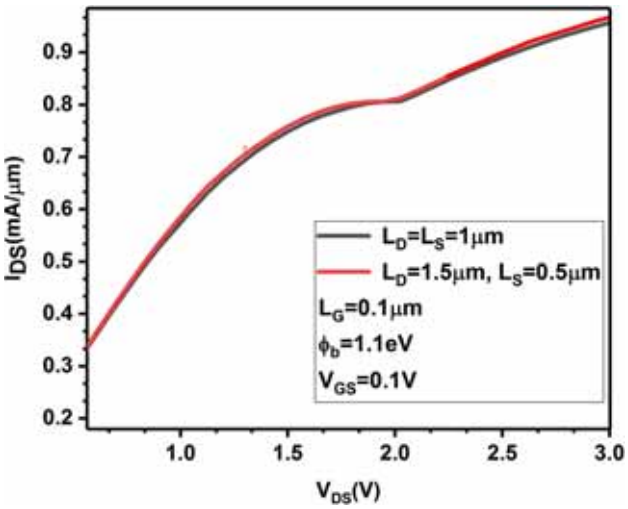

Figure 9. I_{DS}–V_{DS} graph for DC HEMT with back-barrier at different drain and source lengths.

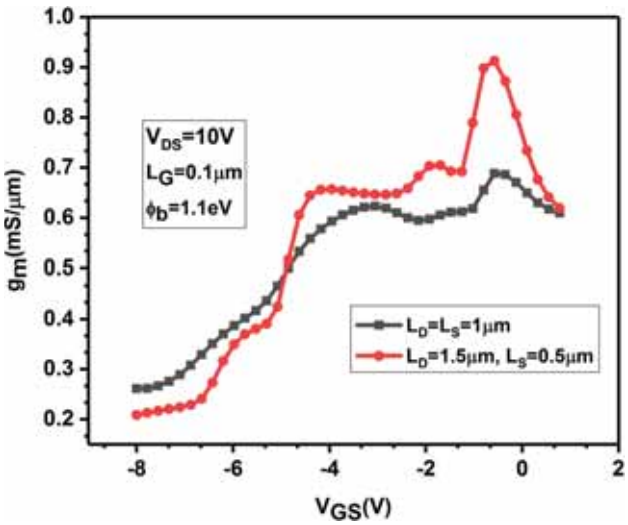

Figure 10. g_m–V_{GS} graph for DC HEMT with back-barrier at different drain lengths and source lengths.

C_{GD}–V_{GS} graph for the heterostructures at $V_{GS} = 10$ V. It is observed that parasitic capacitances increase in the case of DC HEMTs. The charge at the metal/AlGaN interface increases due to increase in sheet charge density in the quantum well for DC HEMT and the capacitances is directly proportional to the charge. So parasitic capacitance increases [26].

$$f_T = \frac{g_m}{2\pi (C_{GS} + C_{GD})}. \quad (1)$$

Figure 8 shows the f_T–V_{GS} graph for the heterostructures. The maximum cut-off frequency for DC with back-barrier is 228 GHz at $V_{GS} = 10$ V. For a DC HEMT, the cut-off frequency increases from 218 to 228 GHz.

Figure 9 shows the I_{DS}–V_{DS} graph for DC HEMT with back-barrier at different drain and source lengths. In the modified device, the drain length is increased and source length is reduced keeping the drain-to-source length unchanged. The drain current is more for the modified device because on changing the contact lengths, the ohmic contact area also changes. The variation in doping region near the contacts reduce the notch height and there is an increase in flexible movement of charge carriers.

Figure 10 shows the g_m–V_{GS} graph for DC HEMT with barrier at different drain and source contact lengths. The transconductance improves when the drain contact length is increased as on increasing the drain contact length there is an increase in flexible movement of

charge carriers and thus the gate control over the channel improves.

Figure 11 shows the f_T–V_{GS} graph for DC HEMT with back-barrier at different drain and source contact lengths. The maximum transconductance and cut-off frequency measured for the modified device of DC HEMT with back-barrier is 0.91 mS/μm and 260 GHz respectively.

Figure 12 shows the I_{DS}–V_{DS} graph for SC HEMT at different gate lengths. The drain current increases when gate length is reduced. The surface roughness scattering and the resistance reduce when the gate length is reduced. So the mobility of the charge carriers and current increase [27].

Figure 13 represents the conduction band energy diagram for different thicknesses of AlGaN barrier. Figure 14 shows the g_m–V_{GS} graph for SC HEMT with varying thickness of the AlGaN barrier (d). When the thickness of the AlGaN barrier increases, the sheet charge density and height of the quantum well increase [28] and control of gate voltage over the channel decreases as transconductance decreases [29].

Figure 15 shows the g_m–V_{GS} graph for DC HEMT with different mole fractions (x) for lower AlGaN layer. For a DC HEMT, a double hump structure is formed in the transconductance graph. It is due to the gate modulation of the upper and lower channel respectively. It is observed that the transconductance decreases when

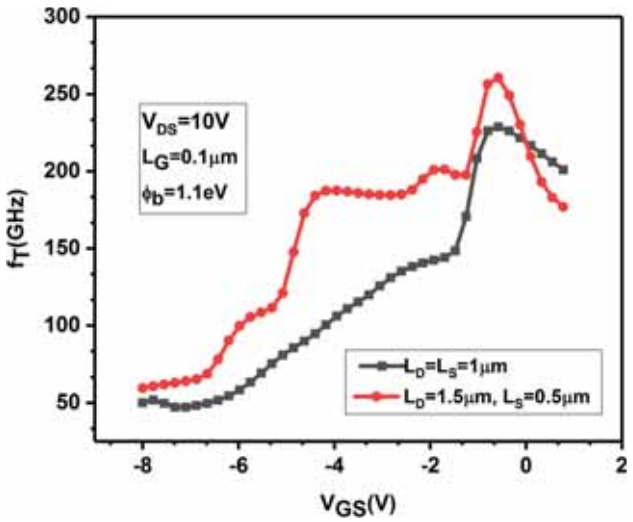

Figure 11. f_T–V_{GS} graph for DC HEMT with back-barrier at different drain length and source lengths.

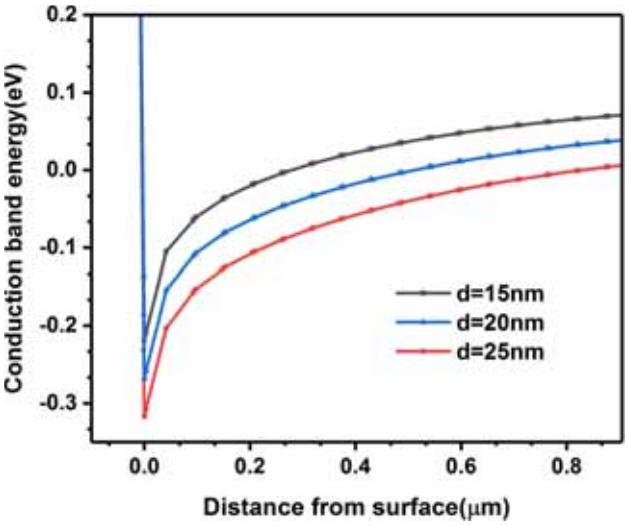

Figure 13. Conduction band energy diagram for different thicknesses of AlGaN barrier in SC AlGaN/GaN HEMT.

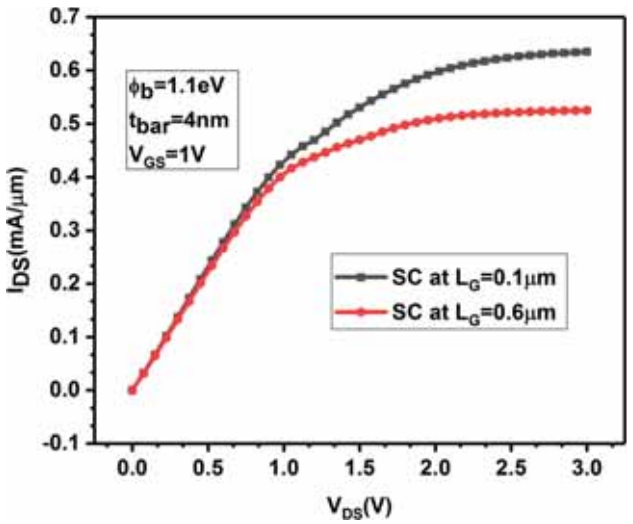

Figure 12. I_{DS}–V_{DS} graph for SC HEMT at different gate lengths (L_G).

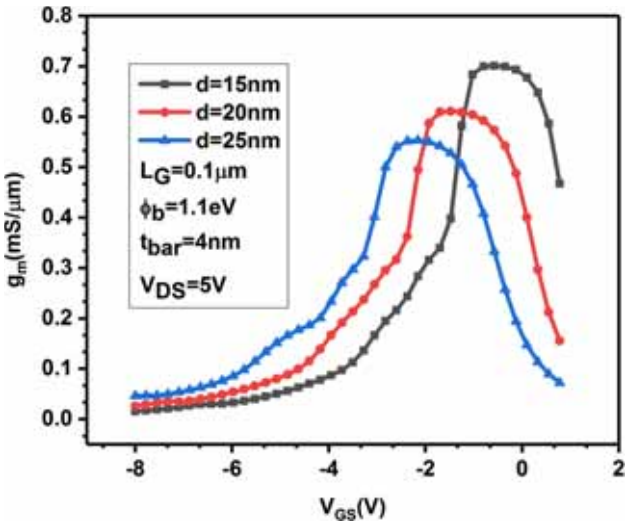

Figure 14. g_m–V_{GS} graph for AlGaN/GaN SC HEMT with different thicknesses of AlGaN barrier (d).

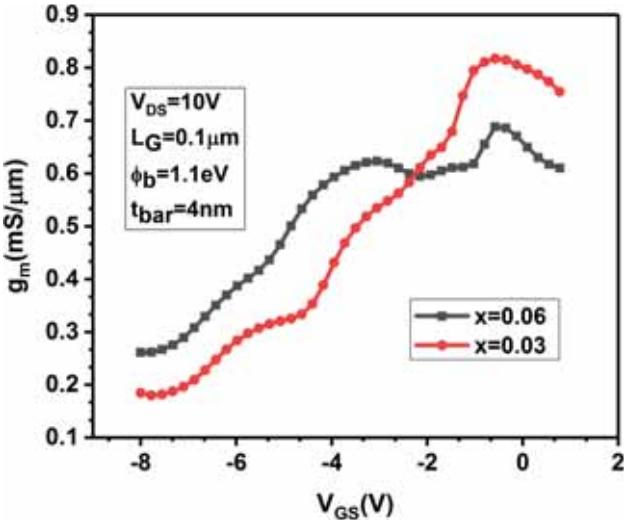

Figure 15. g_m–V_{GS} graph for DC HEMT with different mole fractions for lower AlGaN layer ($Al_xGa_{1-x}N$).

the mole fraction increases because higher mole fraction leads to higher electron density formed in the channel and as a result the gate has less control over the channel as it is difficult for the gate to modulate high electron concentration.

4. Conclusion

In this paper we have studied the SC and DC AlGaN/GaN HEMTs. The performance of the HEMTs improves when a back-barrier is inserted. The DC HEMT with back-barrier exhibits a maximum transconductance of 0.68 mS/μm and a cut-off frequency of 228 GHz at $V_{DS} = 10$ V. The DC HEMT with back-barrier is further modified to get 32.55% improvement in transconductance and 14.03% improvement in cut-off frequency at a gate-to-source voltage of -0.5 V when L_D:$L_S = 3$ compared to the condition when L_D:$L_S = 1$ while keeping drain-to-source spacing unchanged.

Acknowledgement

The authors would like to express their special thanks to School of Electronics Engineering, Kalinga Institute of Technology, Bhubaneswar, India for giving them the necessary laboratory facilities to perform their research work.

References

[1] M Kameche and N V Drozdovski, *Microwave J.* **48(5)**, 164 (2005)
[2] H Arabshahi, *Braz. J. Phys.* **39(1)**, 35 (2009)
[3] S H Park and S L Chuang, *Phys. Rev. B* **59(7)**, 4725 (1999)
[4] H Morkoc, *Electronic and optical processes in nitrides* (Wiley, 2009) Vol. 2
[5] O Ambacher *et al*, *J. Appl. Phys.* **85(6)**, 4725 (1999)
[6] R Quay, *Gallium nitride electronics* (Springer Science and Business Media, 2008) Vol. 96
[7] J Xie *et al*, *Appl. Phys. Lett.* **91(13)**, 132116 (2007)
[8] R S Pengelly *et al*, *IEEE Trans. Microwave Theory Tech.* **60(6)**, 1764 (2012)
[9] T Palacios *et al*, *IEEE Electron Device Lett.* **27(1)**, 13 (2006)
[10] I P Smorchkova *et al*, *IEEE Trans. Microwave Theory Tech.* **51(2)**, 665 (2003)
[11] S Nakamura and T Mukai, *Jpn. J. Appl. Phys.* **31(10B)**, L1457 (1992)
[12] G Simin *et al*, *Jpn. J. Appl. Phys.* **40(11A)**, L1142 (2001)
[13] T Palacios *et al*, *Phys. Status Solidi A* **203(7)**, 1845 (2006)
[14] C Nguyen, N X Nguyen and D E Grider, *Electron. Lett.* **35(16)**, 1380 (1999)
[15] I Daumiller, D Theron, C Gaquière, A Vescan, R Dietrich, A Wieszt, H Leier, R Ventury, U K Mishra, I P Smorchkova, S Keller, N X Nguyen, C Nguyen and E Kohn, *IEEE Electron Device Lett.* **22(2)**, 62 (2001)
[16] R Chu *et al*, *IEEE Trans. Electron Devices* **52(4)**, 438 (2005)
[17] A Kamath *et al*, *IEEE Electron Device Lett.* **33(12)**, 1690 (2012)
[18] M L Schuette *et al*, *IEEE Electron Device Lett.* **34(6)**, 741 (2013)
[19] J W P Hsu *et al*, *Appl. Phys. Lett.* **81(1)**, 79 (2002)
[20] M Asif Khan *et al*, *Appl. Phys. Lett.* **76(25)**, 3807 (2000)
[21] W Lu, V Kumar, R Schwindt, E Piner and I Adesida, *Solid State Electron.* **46(9)**, 1441 (2002)
[22] O Ambacher *et al*, *J. Phys.: Condens. Matter* **14(13)**, 3399 (2002)
[23] J P Ibbetson, P T Fini, K D Ness, S P DenBaars, J S Speck and U K Mishra, *Appl. Phys. Lett.* **77(2)**, 250 (2000)
[24] G Sabui *et al*, *AIP Adv.* **6(5)**, 055006 (2016)
[25] I Khalil, E Bahat-Treidel, F Schnieder and J Wurfl, *IEEE Trans. Electron Devices* **56(3),** 361 (2009)
[26] W Xin-Hua *et al*, *Chin. Phys. B* **19(9)**, 097302 (2010)
[27] G H Jessenet *et al*, *IEEE Trans. Electron Devices* **54(10)**, 2589 (2007)
[28] G Longobardi *et al*, *International Semiconductor Conference* (CAS 2012) (Sinaia, Romania, 2012) Vol. 2
[29] A G Gudkov *et al*, *Proceedings of the Scientific-Practical Conference* "*Research and Development* 2016" (Springer, 2018)